AIAA JOURNAL
Vol. 41, No. 7, July 2003

Shock/Vortex Interactions Induced by Blast Waves

S. M. Liang* and C. P. Lo†
National Cheng-Kung University, Tainan 701, Taiwan, Republic of China

The problem of blast-wave propagation in an open-ended duct with a 90-deg sharp convex (expansion) corner is numerically investigated by the use of a high-resolution Euler solver. The complicated flowfields induced by the blast-wave diffraction around the corner and by a secondary shock/vortex interaction are explored. Both a two-dimensional case and an axisymmetric case are considered. It is found that two vortices near the corner in the two-dimensional case (or two ring vortices in the axisymmetric case) are induced by the blast-wave diffraction. One vortex is stronger and is located farther downstream than the other. These two vortices rotate in opposite directions. In the axisymmetric flow, the major ring vortex is located farther downstream than that for the corresponding two-dimensional case, resulting in a lower pressure at the vortex centers. This is due to the relieving effect that is represented by an extra nonvanishing term in the vorticity transport equation in the axisymmetric case. The trajectories of the major planar vortex or ring vortex induced by different blast intensities are explored. Basically, the planar major vortex (or the major ring vortex in the axisymmetric case) moves downstream before a critical time and then turns toward the duct centerline after the critical time. The critical time roughly corresponds to the formation of a minor vortex.

Introduction

SHOCK/VORTEX interaction is identified as a major noise source and has become an important engineering research topic in recent years. Blast waves take place in exhaust pipes of internal combustion engines, in buildings during explosions, and in explosions for penetration of blast waves into protective structures. A blast wave has the property of a shock front accompanied by expansion waves, and one or more secondary shock waves may follow behind the expansion waves. The flow structures induced by a blast wave and by a blast-wave/vortex interaction around a sharp convex (expansion) corner might be different from those induced by a shock wave around the corner. The objective of this numerical study is to understand the basic flow structures induced by weak blast waves and the associated shock/vortex interactions.

There have been many papers that reported the basic flow structure induced by shock wave diffraction around a sharp edge or corner. Howard and Mathews[1] studied experimentally the fundamental flow structure induced by shock wave diffraction. The basic induced flow structure consisted of expansion waves, a slip line, a contact surface, and vortices. The review paper of Bazhenova et al.[2] provided an explanation of the unsteady interactions of shock wave propagation, which included the shock wave diffraction around an expansion corner. Hillier[3] studied computationally the vortex generation due to shock wave diffraction around a 90-deg sharp convex edge. He used an explicit method of a second-order Godunov scheme. The study of Mandella et al.[4] indicated that the vortices near the corner were generated due to a baroclinic effect, assuming inviscid flow. Yang et al.[5] conducted a series of experiments to obtain some holographic interferograms for shock wave diffraction around a 90-deg sharp convex corner at various shock Mach numbers. Uchiyama and Inoue[6] explored numerically the evolution of a corner vortex by an adaptive mesh refinement algorithm.

The problem of shock/vortex interaction has been a subject in the development of future supersonic and hypersonic transport aircraft. Andreopoulos et al.[7] reviewed what is currently understood regarding the shock wave/turbulence interaction. Grönig[8] presented a paper that reviewed current knowledge and progress on the problem of shock/vortex interaction. Dosanjh and Weeks[9] studied experimentally a columnar shock-starting vortex that interacted with a reflected normal shock in a shock tube. Haas and Sturtevant[10] investigated experimentally the interaction of a weak planar shock wave with cylindrical and spherical gas inhomogeneities. They found a vortical flow structure induced by the flow inhomogeneity. Later, Picone and Boris[11] studied theoretically the vorticity generation induced by a shock/gas bubble interaction. Jacobs[12] studied experimentally and quantified the mixing induced by the interaction of a normal shock wave with a cylindrical volume of light gas. He found that rapid mixing resulted from flow motion induced by vorticity. At the same time, Yang et al.[13] investigated analytically and computationally the vortical flow induced by the interaction of a planar shock wave and a planar light-gas jet. They pointed out that the vorticity generated is mainly due to the misalignment of the pressure and density gradients. Cetegen and Hermanson[14] investigated the instability mechanics and mixing enhancement arising from the interaction of a compressible vortex ring with a normal shock wave. Ellzey and Henneke[15] investigated experimentally a shock/vortex interaction and showed that the interaction could produce a primarily quadrapolar acoustic wave with a strong compression behind the shock front. Grasso and Pirozzoli[16] studied numerically the shock and vortex deformations and the mechanism of sound generation. The numerical method used was a weighted essentially nonoscillatory (ENO) scheme for solving the Euler equations.

In this study, the problem of a planar blast wave propagating in an open-ended duct with a 90-deg sharp convex corner at its exit is considered. The working fluid is air. The planar blast wave is generated by the rupture of diaphragms that separate an upstream rectangular high-pressure p_h region with the density ρ_h from two low-pressure p_l regions with the density ρ_l in the duct, as shown in Fig. 1. The centerline of the high-pressure region with a width of $0.008R$ is located at $x = 0.12R$, where R is one-half of the width of the duct. Two planar blast waves are generated. One blast wave propagates downstream, which is of interest in this study; the other propagates upstream. The left-traveling blast wave will not be reflected because of the assumption of no far left wall. The right-traveling blast wave has a primary shock wave, followed by expansion waves and a secondary shock, resulting in a shock/vortex interaction around the corner. The primary shock wave can induce vortices as it diffracts around the corner, and the subsequent secondary shock will then interact with the induced vortices. Both cases of two-dimensional and axisymmetric flows are examined and compared. In the axisymmetric case, a vortex ring is induced by the primary shock,

Received 18 July 2001; revision received 12 June 2002; accepted for publication 4 February 2003.

*Professor, Institute of Aeronautics and Astronautics. Associate Fellow AIAA.
†Graduate Student. Institute of Aeronautics and Astronautics.

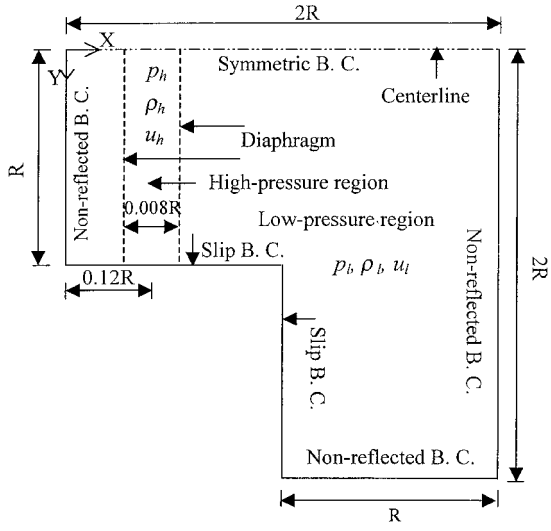

Fig. 1 Schematic for blast-wave generation and computational domain with boundary conditions.

unlike the planar vortex induced in the two-dimensional case. A high-resolution Euler solver was developed for our numerical simulation. A fifth-order weighted, essentially nonoscillatory, scheme of Jiang and Shu[17] was used for spatial discretization, as was a fourth-order Runge–Kutta method for time integration. The present study will pave the way for further studies of noise generation and mixing due to blast/vortex interactions.

Mathematical Model and Numerical Method

Assume that the flow is inviscid and that there is no external force. The assumption of inviscid flow is validated by the experimental data of Yang.[18] His experimental data show that the vortices, due to the shear layer, are relatively small compared with those induced by the diffracted shock wave. The equations governing blast-wave propagation in the open-ended duct are the continuity, momentum, and energy equations. Thus, the Euler equations are solved numerically in this study.

The numerical method of the high-order scheme of Jiang and Shu[17] in a finite volume approach, with an extension to curvilinear coordinates, is used for solving the Euler equations. Namely, a fourth-order Runge–Kutta method is used for time integration and a fifth-order weighted ENO scheme[17] is used for spatial discretization. Initially, a blast wave of interest is produced that propagates downstream into a region of quiescent ambient (undisturbed) air at a pressure of $p_l = 1$ atm. The boundary condition imposed on the duct wall is the tangency condition. At the upstream boundary of the duct and the downstream boundary, the nonreflecting boundary condition by Thompson[19] is specified, as shown in Fig. 1. Because only one-half of the computational domain was used for saving computer memory and computational time, a symmetry condition is imposed on the centerline. The Courant number is chosen to be 0.5. The minimum number of local time steps over the computational domain is used for unsteady flow calculations. Namely, a global time step is used at each time step.

Results and Discussion

Code Validation

To validate the present Euler solver, the problem of planar shock wave diffraction around a 90-deg sharp convex (expansion) corner is tested. The working fluid is helium ($\gamma = 1.67$). Our computed result is compared with the two-dimensional holographic interferograms of Yang[18] for two shock Mach numbers, 1.5 and 2.02. Only the case of $M_s = 1.5$ is shown in this study. Figure 2 shows the comparison of the computer holograph with the experimental result at $M_s = 1.5$ and $\bar{t} = 55\ \mu$s. Time $\bar{t} = 0$, as in Ref. 18, corresponds to the time of the shock arrival at the corner at $x = 3$. Note that the computational time t is dimensionless and is defined as $t = \bar{t}R/V_s$, where R and

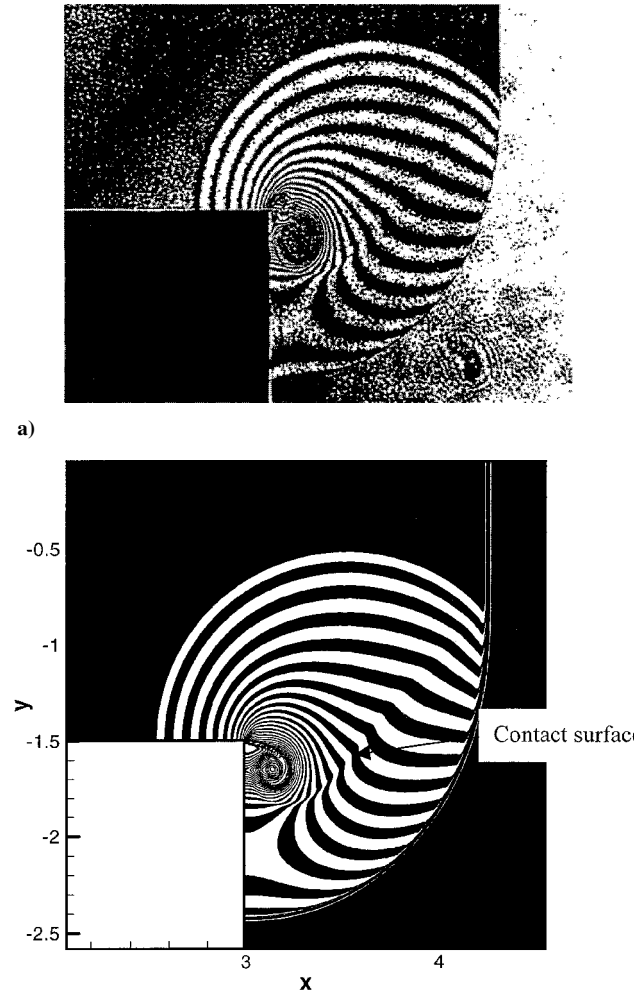

Fig. 2 Comparison of a) the holographic interferogram with b) the computer holograph for planar shock wave diffraction around a 90-deg sharp convex corner, $M_s = 1.5$, $\bar{t} = 55\ \mu$s, and $\Delta\rho = 0.0514$ kg/m^3 (or 0.046, dimensionless).

V_s denote the one-half duct width and shock velocity, respectively. Moreover, the density is nondimensionalized by the density ρ_l of the undisturbed fluid. Note the contact surface (CS) and the induced vortex in the computer holograph. The CS separates the flow that has been compressed by the diffracted shock wave from the flow that has been expanded around the corner. The flow entropy behind the incident shock wave is higher than that behind the diffracted shock wave because the diffracted shock wave is weaker than the incident shock wave. The entropy of the expanded flow on the left-hand side of the CS has the same value as that of the flow behind the incident shock wave because of the isentropic process of flow expansion for an inviscid flow. From Fig. 2, it is evident that qualitative agreement is obtained. For the quantitative comparison, when the incident shock Mach numbers at the corner are 1.5 and 2, our computed wall shock Mach numbers after diffraction are 1.12 and 1.26, which agree well with the experimental values of 1.15 and 1.3 (Ref. 20). In these two cases, the working fluid is air.

Effect of Grid Number

To make sure that the numerical solution obtained is independent of grid number, four uniform grids, 200×200 (grid 1), 300×300 (grid 2), 400×400 (grid 3), and 500×500 (grid 4) are used for the two-dimensional problem of blast-wave propagation with $p_h/p_l = 50$. We recorded the maximum and minimum wall pressures beneath the corner. We plotted the changes of the maximum and minimum wall (dimensionless) pressures with the grid number. It was found that the minimum wall pressure is the same value of

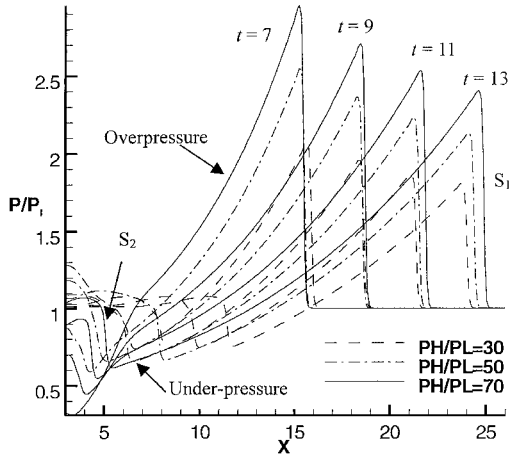

Fig. 3 Pressure profiles of planar blast waves produced with different pressure ratios (p_h/p_l) at different instants for the two-dimensional case.

0.707 for grids 2, 3, and 4. The change of maximum wall pressure is −12% when grid 1 is changed to grid 2, −7.2% for grid 2 to 3, and −5.4% for grid 3 to 4. Thus, the uniform grid of 500 × 500 with spacing, $\Delta x = \Delta y = 0.1$, is used to save computer memory and computation time because numerical computations are performed on a personal computer, a Pentium III-800 with 512 MB of memory.

Flowfield Induced by Unsteady Blast Wave

First, we will consider the two-dimensional problem of blast-wave propagation. In the next section, we will discuss the corresponding axisymmetric problem and compare both cases. To produce different intensities of blast waves, the pressure ratios are set to be $p_h/p_l = 30$, 50, and 70 so that the blast-wave front has a shock Mach number M_s ranging from 1.3 to 1.5 at the corner. To do that, the centerline of the high pressure, with a width of 0.2, is chosen to be located at $x = 3$. The sharp corner is properly arranged at $x = 24.9$, so that the primary shock front of the blast wave produced will have a shock Mach number of about 1.4 at the sharp corner for $p_h/p_l = 50$. Namely, one can adjust the corner location to control the blast-wave intensity at the corner if the high-pressure region is fixed at upstream. Alternatively, we adjust the high-pressure region location to obtain the desired blast intensity at the corner if the corner location is fixed. In this study, the former approach is taken. The lower wall of the duct is located at $y = -25$. Figure 3 shows the generated blast-wave pressure profiles at various instants ($t = 7, 9, 11$, and 13) for different pressure ratios. The computational time t is a dimensionless time as defined before. The blast waves produced are composed of a shock front S_1, the primary shock, followed by expansion waves, and, subsequently, a secondary shock wave S_2. There are two phases in the pressure profile. One is the positive phase of overpressure and the other is the negative phase of underpressure. At $t = 13$, the blast wave produced has an approximate shock Mach number of $M_s = 1.3$ near the sharp corner for the case of $p_h/p_l = 30$, $M_s = 1.4$ for $p_h/p_l = 50$, and $M_s = 1.5$ for $p_h/p_l = 70$. Later on, the primary shock starts to diffract around the corner. The shock diffraction induces a vortex behind the diffracted shock wave D_1. From Fig. 3, note that these primary shock fronts decay nonlinearly and very quickly with time.

Figure 4 shows the density, pressure, and vorticity contours near the corner at $t = 24$ for $p_h/p_l = 50$. In Fig. 4a, note the two contact surfaces, which are already developed upstream. The two contact surfaces are located at about $x = 1.3$ and 4.7, respectively. From Figs. 4a and 4b, note the expansion wave front induced by the shock diffraction, around the corner. At this instant, a newly formed vortex is also developed. We can see the two vortices (V_1 and V_2) generated around the corner, as shown in Fig. 4c. The major vortex V_1 is located farther downstream than the secondary minor vortex V_2. It is evident that the major vortex is stronger than the minor vortex. The major vortex rotates in a clockwise direction with positive values of vorticity, and the minor vortex rotates in a counterclockwise

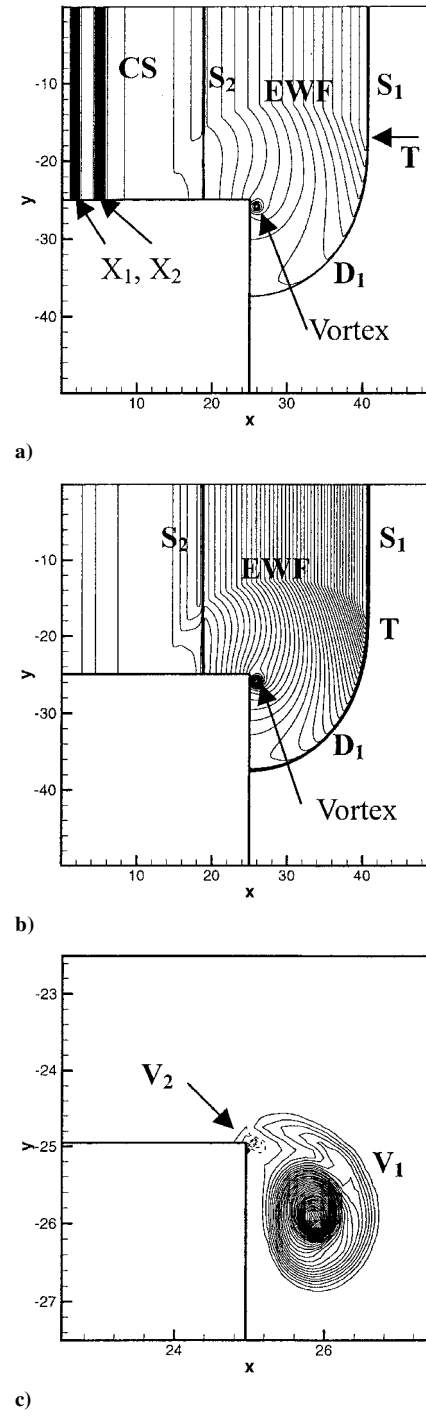

Fig. 4 Planar blast-wave diffraction at $t = 24$: a) density, b) pressure, and c) vorticity contours, $p_h/p_l = 50$ (two-dimensional case).

direction with negative values of vorticity. The centers of the two vortices exhibit local low-pressure regions, as expected. Notice that in Fig. 4 (and hereafter) the locations of the duct walls are not the real wall locations and are shifted by a distance of 0.05 to the real wall location. This is due to the use of a finite volume approach in which flow properties are defined at the cell centers. We did not have a special treatment on the real wall location in plotting.

This vorticity ω production of these two vortices is governed by the vorticity transport equation:

$$\frac{\mathrm{D}\omega}{\mathrm{D}t} = -\omega(\nabla \cdot \boldsymbol{V}) - \frac{\nabla p \times \nabla \rho}{\rho^2} \tag{1}$$

where the vorticity vector ω is the curl of the velocity $\boldsymbol{V}$, or $\omega = \nabla \times \boldsymbol{V}$, which is perpendicular to the flow plane, and where

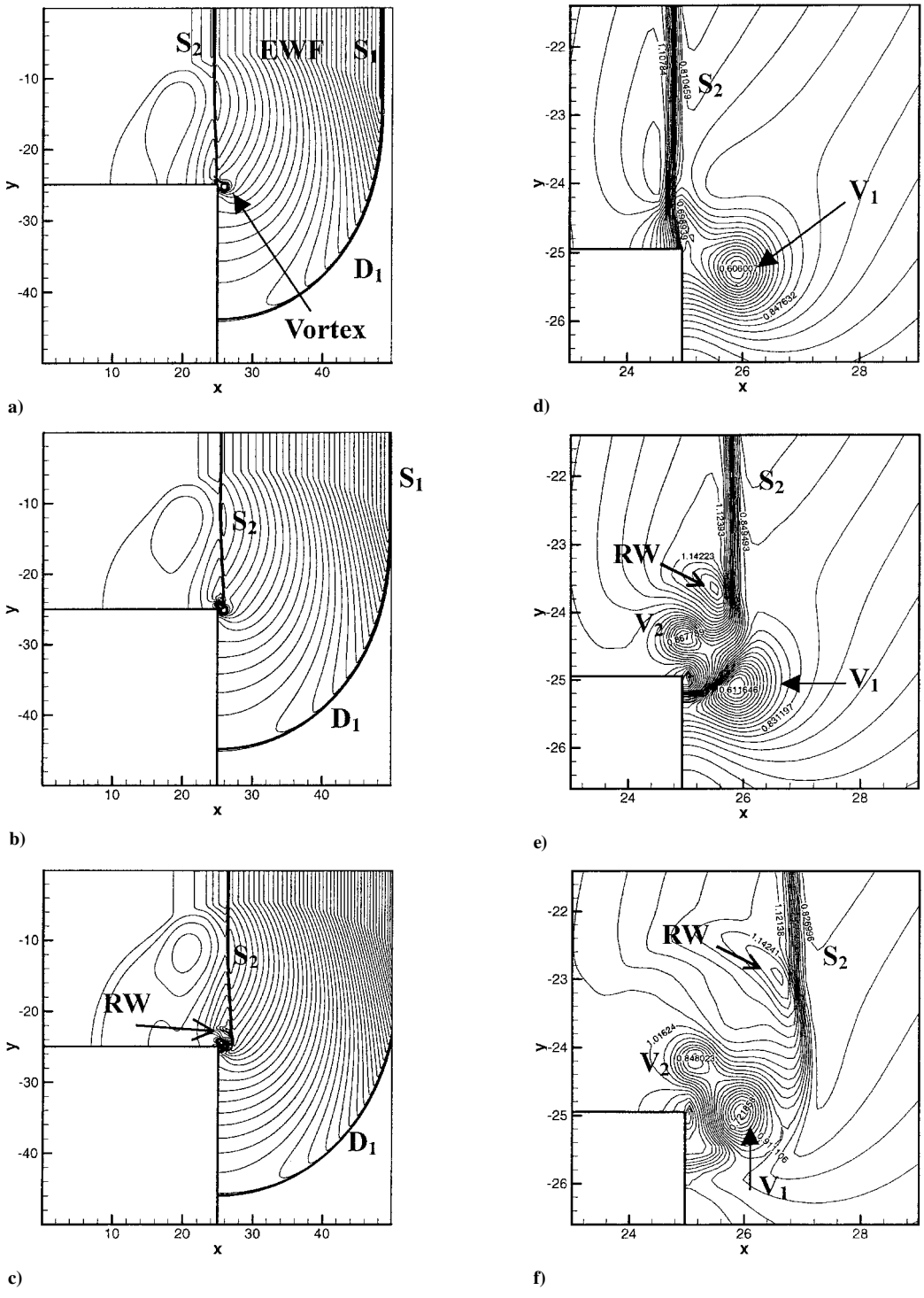

Fig. 5 Pressure contours at different instants, $p_h/p_l = 50$: a and d) $t = 31$; b and e) $t = 32$; and c and f) $t = 33$ for planar blast/vortex interaction; a–c) global flowfields and d–f) local flowfields.

∇ is the two-dimensional gradient operator. Equation (1) states that the vorticity production is affected by the vorticity itself, multiplied by fluid dilation ($\nabla \cdot \boldsymbol{V}$) and by the baroclinic effect of misalignment of the density and pressure gradients. It was found that the baroclinic effect is dominant in the vorticity production during and after the secondary shock/vortex interaction, compared with the term $-\omega(\nabla \cdot \boldsymbol{V})$.

Planar Shock/Vortex Interaction

At $t = 31$, the secondary shock has arrived at the convex corner and starts to interact with the vortex induced by the primary shock (S_1, D_1), as shown in Figs. 5a and 5d. In Fig. 5d, we can clearly see the pressure contours in the major vortex V_1. The dimensionless pressure, normalized by p_h, is 0.606 at the vortex center. Because of the influence of the secondary shock S_2, the minor vortex is not seen in Fig. 5d. At $t = 32$, the secondary shock S_2 is located between the two vortices (V_1 and V_2) and interacts with them, as shown in Figs. 5b and 5e. The two vortices result in two local low-pressure regions at their centers. The vorticities of these two vortices (V_1 and V_2) are shown in Fig. 6. From Fig. 6, we can clearly see the two vortices, which rotate in an opposite direction. The major vortex V_1 has a vorticity value of 3.04 at its center, whereas the minor-vortex center has a value of -0.59. At this instant, the secondary shock just

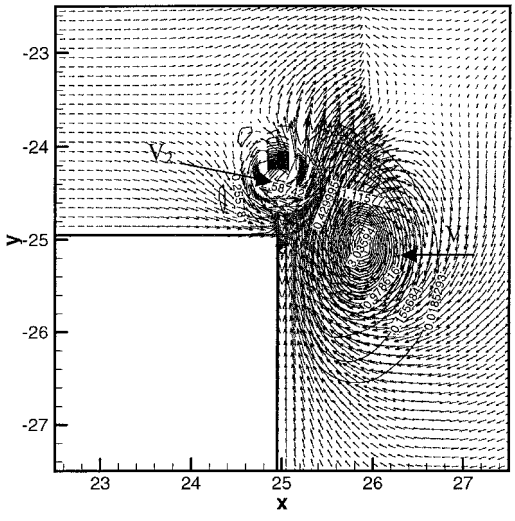

Fig. 6 Vorticity contours and velocity field for planar blast/vortex interaction at $t = 32$ and $p_h/p_l = 50$.

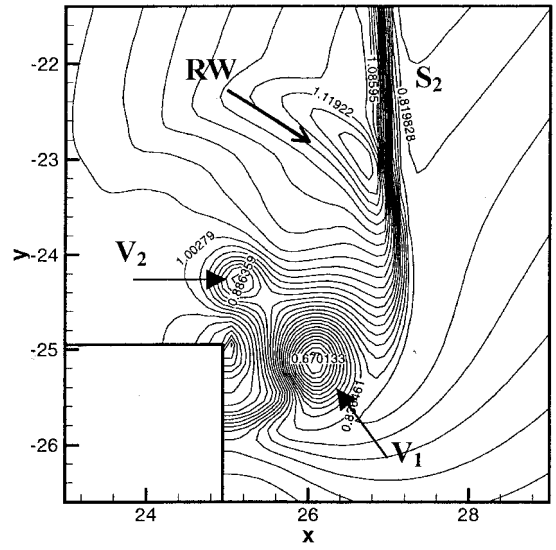

Fig. 7 Secondary shock/vortex interaction for the axisymmetric case, $p_h/p_l = 50$ and $t = 33$.

passed the minor vortex and produced a reflected shock wave. The pressure at the major-vortex center is 0.612, and at the minor-vortex center it is 0.868. Because of the mutual influence of the secondary shock on the major vortex, the lowest pressure of the major vortex is increased from 0.606 at the preceding instant, to 0.612, about a 1% increase. At $t = 33$, the secondary shock has passed the two vortices, and the pressure at the major-vortex center has increased from 0.612 before interaction to 0.722 after interaction, about an 18% increase. However, the pressure at the minor-vortex center is decreased from 0.868 to 0.848, about a 2.3% decrease. The corresponding vorticity at the vortex center for the minor vortex is slightly changed from -2.59 at $t = 32$ to -2.65 at $t = 33$. For the major vortex, the center vorticity is also slightly increased from 3.04 to 3.13. This implies that the passing of the secondary shock does not have influence on the growth of the minor and major vortices.

Comparison of Two-Dimensional Case with Axisymmetric Case

Consider an axisymmetric flow that corresponds to the preceding two-dimensional blast-wave diffraction problem. It is obvious that the induced vortices in the axisymmetric case are vortex rings instead of planar vortices, as in the two-dimensional case. In the axisymmetric flow, the flow velocity and vorticity are three-dimensional vectors. In the axisymmetric problem, the vorticity production is given by

$$\frac{\mathrm{D}\omega}{\mathrm{D}t} = -\omega(\nabla \cdot \boldsymbol{V}) - \frac{\nabla p \times \nabla \rho}{\rho^2} + (\omega \cdot \nabla)\boldsymbol{V} \qquad (2)$$

The difference between Eqs. (1) and (2) is the term $(\omega \cdot \nabla)\boldsymbol{V}$. In the two-dimensional case, the term $(\omega \cdot \nabla)\boldsymbol{V}$ vanishes because the vorticity vector ω is perpendicular to the flow plane. However, it is not zero in the axisymmetric case. We plotted the pressure contours at $t = 31$, 32, and 33, which were very similar to those shown in Fig. 5. To be succinct, we omit these results at $t = 31$ and 32 and only show the result at $t = 33$. It was found that the pressure at the major-vortex center is 0.583 at $t = 31$ in the axisymmetric case, which is slightly lower than that (0.606) in the corresponding two-dimensional case. The pressure difference for these two cases is only about 4%. Figure 7 shows the local flowfields around the corner after the secondary shock/vortex interaction ($t = 33$). The pressure at the major-vortex center is 0.67, which is about 7.2% lower than that (0.722) in the corresponding two-dimensional case. However, the pressure at the minor-vortex center is 0.866, which is higher than that (0.848) in the corresponding two-dimensional case. Comparing the pressures at the major-vortex center before and after the secondary shock/vortex interaction, we find that the pressure is increased by 15% for the axisymmetric case, and 12% for the two-dimensional case. In conclusion, the pressures at the major ring vortex centers

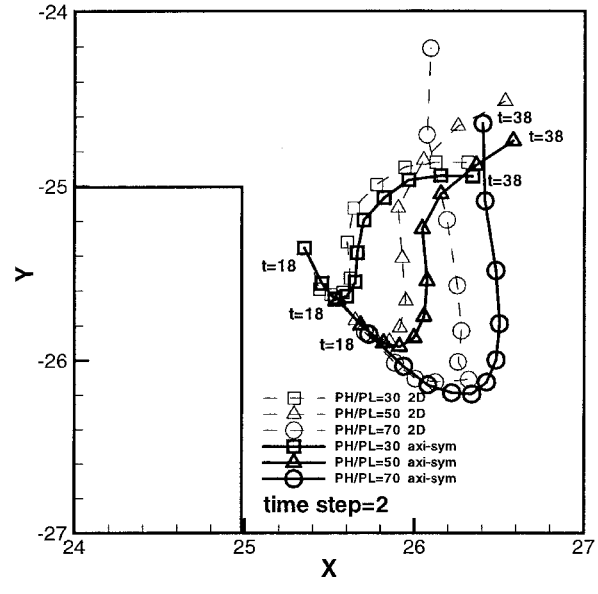

a)

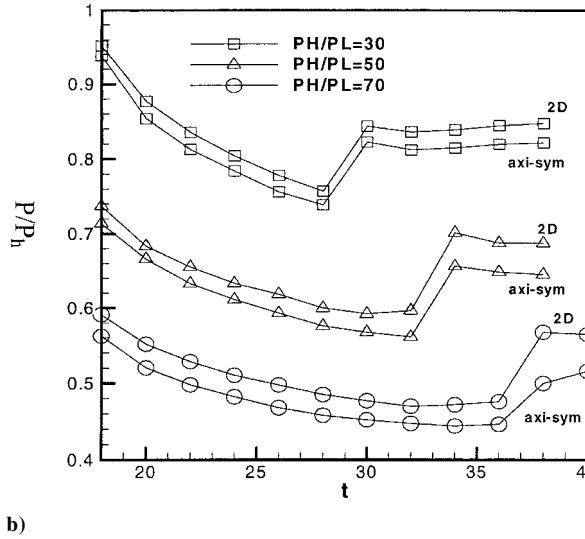

b)

Fig. 8 Comparison of a) the trajectories of the major planar vortex and major ring vortex centers and b) the corresponding pressures at major vortex centers from $t = 18$ to 38, with $\Delta t = 2$ for different blast intensities.

are lower than that for the corresponding two-dimensional case. We believed that this is due to a relieving effect for a three-dimensional problem, resulting in a stronger vortex and, consequently, a lower pressure at the vortex center for the axisymmetric case. The relieving effect is represented by the extra nonvanishing term, $(\omega \cdot \nabla)\boldsymbol{V}$, in the vorticity transport equation (2) for the axisymmetric case.

Figure 8a shows the trajectories of the centers of the major vortices induced by different blast intensities in the two-dimensional and axisymmetric cases during the period of $t = 18$–38. It is found that there is a critical time t_c for the induced vortex to move toward the centerline. The critical time roughly corresponds to the formation of the secondary, minor vortex around the corner. Namely, the mutual influence of the two vortices leads to the upward movement of the major vortex. The critical time t_c is about $t_c = 22$ for the case of $p_h/p_l = 30$, $t_c = 24$ for $p_h/p_l = 50$, and $t_c = 26$ for $p_h/p_l = 70$. Generally, the vortex trajectories for the two-dimensional and axisymmetric cases are not very different. The vortex center is moved farther downstream before the critical time for stronger blast waves. The ring vortices are located slightly farther downstream than the planar vortices.

Figure 8b shows the dimensionless pressures at the major vortex centers for different blast intensities. It is found that the pressure at the vortex center decreases with time until the secondary shock wave arrives and interacts with the vortex. The influence of the secondary shock causes a pressure jump as indicated in Fig. 8b. After the passage of the secondary shock, the pressures in the vortical regions change slightly. From Fig. 8b, one can see that the center pressures in the major ring vortex for the axisymmetric case are lower than those for the two-dimensional case. The pressure differences can be explained by the relieving effect, as mentioned earlier. The pressure differences are almost constant, as shown in Fig. 8b. This implies that the term $(\omega \cdot \nabla)\boldsymbol{V}$ enhances the vortex strength in the axisymmetric case, resulting in lower pressures at major vortex centers.

Conclusions

The high-resolution Euler solver is verified to simulate accurately the flowfields induced by a planar blast wave diffracting around a 90-deg sharp convex corner and by planar and axisymmetric shock/vortex interactions. It is found that the primary shock wave can induce a stronger (major) vortex and a weaker (minor) vortex near the convex corner for the two-dimensional problem. In the axisymmetric problem, two ring vortices are generated. The major planar vortex (in the two-dimensional case) or ring vortex (in the axisymmetric case) is located farther downstream than the minor vortex. The major vortex rotates in a clockwise direction that is opposite to the rotating direction of the minor vortex. In the axisymmetric case, the pressures at the major vortex centers are lower than that for the corresponding two-dimensional case. This can be explained by the relieving effect that is represented by the extra nonvanishing term in the vorticity transport equation in the axisymmetric case. The intensity of the blast wave can greatly influence the induced vortex strength, resulting in the development of low-pressure regions. For the two-dimensional and axisymmetric cases, because of the mutual influence of the secondary shock/vortex interaction, the interaction results in a pressure increase at the major vortex center and a pressure decrease at the minor vortex center after the interaction. However, the interaction has no influence on the growth of these two vortices. A similar situation occurs in the axisymmetric case. The time histories of vortex trajectories induced by blast waves with different intensities are explored for the two-dimensional and axisymmetric cases. It is found that the planar major vortex (or the major ring vortex in the axisymmetric case) moves downstream before a critical time and then turns toward the duct centerline after the critical time. The critical time roughly corresponds to the formation of a minor vortex. Moreover, a stronger blast wave induces stronger vortices, positioned farther downstream, than does a weaker blast wave. Because of the relieving effect, stronger vortices induced by blast-wave diffraction result in lower-pressure regions at vortex centers in the axisymmetric case, compared with those in the corresponding two-dimensional case.

Acknowledgments

The support of this work under National Science Council Contract 89-2612-E-006-018 is gratefully acknowledged. The authors thank J. Yang for his provision of Fig. 2a. The authors also thank the reviewers for their valuable comments and suggestions and K. Jansma for reading the manuscript.

References

[1]Howard, L., and Mathews, D., "On the Vortices Produced in Shock Diffraction," *Journal of Applied Physics*, Vol. 27, No. 3, 1956, pp. 223–231.

[2]Bazhennova, T. V., Gvozdeva, L. G., and Nettleton, M. A., "Unsteady Interactions of Shock Waves," *Progress in Aerospace Sciences*, Vol. 21, No. 1, 1984, pp. 249–331.

[3]Hillier, R., "Computation of Shock Wave Diffraction at a Ninety Degrees Convex Edge," *Shock Waves*, Vol. 1, No. 2, 1991, pp. 89–98.

[4]Mandella, M., Moon, Y. L., and Bershader, D., "Quantitative Study of Shock Generated Compressible Vortex Flows," *Shock Waves and Shock Tubes*, edited by D. Bershader and R. Hanson, Stanford Univ. Press, Stanford, CA, 1986, pp. 471–477.

[5]Yang, J., Onodera, O., and Takayama, K., "Holographic Interferometric Investigation of Shock Wave Diffraction," *Visualization Society of Japan*, Vol. 14, Supplement No. 1, 1994, pp. 85–88.

[6]Uchiyama, N., and Inoue, O., "Shock Wave/Vortex Interaction in a Flow over 90-deg Sharp Corner," *AIAA Journal*, Vol. 33, No. 9, 1995, pp. 1740–1743.

[7]Andreopoulos, Y., Agui, J. H., and Briassulis, G., "Shock Wave–Turbulence Interactions," *Annual Review of Fluid Mechanics*, Vol. 32, 2002, pp. 309–345.

[8]Gröing, H., "Shock Wave/Vortex Interaction," *Proceedings of the Second International Workshop on Shock Wave/Vortex Interaction*, Inst. of Fluid Science, Tohoku Univ., Sendai, Japan, 1997, pp. 1–14.

[9]Dosanjh, D. S., and Weeks, T. M., "Interaction of a Starting Vortex as well as a Vortex Street with a Traveling Shock Wave," *AIAA Journal*, Vol. 3, No. 2, 1965, pp. 216–223.

[10]Haas, J.-F., and Sturtevant, B., "Interaction of Weak Shock Waves with Cylindrical and Spherical Gas Inhomogeneities," *Journal of Fluid Mechanics*, Vol. 181, Aug. 1987, pp. 41–76.

[11]Picone, J. M., and Boris, J. P., "Vorticity Generation by Shock Propagation Through Bubbles in a Gas," *Journal of Fluid Mechanics*, Vol. 189, April 1988, pp. 23–51.

[12]Jacobs, J. W., "Shock-Induced Mixing of a Light-Gas Cylindrical," *Journal of Fluid Mechanics*, Vol. 234, Jan.1992, pp. 629–649.

[13]Yang, J., Kubota, T., and Zukoski, E. E., "An Analysis and Computational Investigation of Shock-Induced Vortical Flows," AIAA Paper 92-0316, Jan. 1992.

[14]Cetegen, B. M., and Hermanson, J. C., "Mixing Characteristics of Compressible Vortex Rings Interacting with Normal Shock Waves," *Combustion and Flame*, Vol. 100, No. 2, 1995, pp. 232–240.

[15]Ellzey, J. L., and Henneke, M. R., "The Shock–Vortex Interaction: The Origins of the Acoustic Wave," *Fluid Dynamics Research*, Vol. 21, No. 3, 1997, pp. 171–184.

[16]Grasso, F., and Pirozzoli, S., "Shock-Wave–Vortex Interactions: Shock and Vortex Deformations, and Sound Production," *Theoretical and Computational Fluid Dynamics*, Vol. 13, No. 6, 2000, pp. 421–456.

[17]Jiang, G. S., and Shu, C.-W., "Efficient Implementation of Weighted ENO Schemes," *Journal of Computational Physics*, Vol. 126, No. 1, 1996, pp. 202–228.

[18]Yang, J., "An Experimental and Theoretical Investigation on the Behavior of Weak Shock Waves," Ph.D. Dissertation, Inst. of Fluid Science, Tohoku Univ., Sendai, Japan, April 1995 (in Japanese).

[19]Thompson, K. W., "Time Dependent Boundary Conditions for Hyperbolic Systems," *Journal of Computational Physics*, Vol. 68, No. 1, 1987, pp. 1–24.

[20]Abate, G., and Shyy, W., "Dynamic Structure of Confined Shock Undergoing Sudden Expansion," *Progress in Aerospace Sciences*, Vol. 38, No. 1, 2002, pp. 23–42.

M. Sichel
Associate Editor